Differential Equations and Dynamical Systems
https://doi.org/10.1007/s12591-025-00735-z

ORIGINAL RESEARCH

Cellular Decision Making and Signal Adaptation Via Incoherent Feedforward and Negative Feedback Loops

Necmettin Yildirim[1]

Received: 3 November 2023 / Accepted: 12 August 2025
© Foundation for Scientific Research and Technological Innovation 2025

Abstract
Understanding how cells attenuate responses initiated by external signals and display adaptive dynamics is a fundamental question in biology. This study explores two well-known control mechanisms to gain insights into how cellular signal adaptation occurs in each. The first mechanism involves an incoherent feedforward loop(IFFL), and the second involves a negative feedback loop(NFBL). After deriving the sufficient conditions for the adaptive dynamics of each mechanism, we determine the parameter regime in which adaptation occurs. Mathematical analysis shows that the parameter regime for adaptive dynamics in the IFFL model is broader than that in the NFBL model. Additionally, the relationship between the signal level and the steady state of the intermediate protein is linear in the IFFL model, whereas this relationship is saturating in the NFBL model. Our simulation results show that for the constant prolonged input signals, the IFFL model is faster to produce a response and quicker to return to its pre-steady state compared to the NFBL model when the signal protein has a moderate to high affinity to the response protein. The NFBL model, with low affinity between the signal protein and the response protein, returns to its pre-steady state more quickly, but lacks the capacity to generate a strong response. However, the NFBL model with a high affinity of the signal protein to the response protein is capable of producing a higher maximal response compared to the IFFL model for weaker signals, but this dynamic is not robust against repetitive pulse-type signals.

Keywords Mathematical modeling · Dynamical systems · Computer simulation · Systems biology · Cell signaling · Signal adaptation

✉ Necmettin Yildirim
nyildirim@ncf.edu

[1] Division of Natural Sciences, New College of Florida, 5800 Bayshore Road, Sarasota, FL 34243, USA

Published online: 02 September 2025

Introduction

Cells continuously interact with their environment by receiving signals and generating appropriate responses to maintain homeostasis. In response to persistent signals, cells may exhibit diminished responses over time. This phenomenon, known as adaptation, enables cells to attenuate or terminate their response to prolonged stimulation. Adaptation can be classified into two types: perfect adaptation, in which the system fully returns to its baseline state, and partial adaptation, where the system returns to a state close to baseline after a certain period.

Adaptation is a common feature of many cellular signaling pathways, mediated by various biochemical mechanisms known as network motifs. The most prominent motifs responsible for adaptive dynamics are incoherent feedforward loops(IFFLs) and negative feedback loops(NFBLs). There are four types of IFFL motifs, with Type I IFFLs being the most prevalent in organisms like yeast and E. coli [1]. For example, the IFFL motifs are found in ERK signaling during cell fate decision-making [2–5], RTK signaling in cell-to-cell communication [6–8], and NF-κB signaling in immune responses [2, 9, 10]. The IFFLs are crucial for cellular signal processing and decision-making, serving functions such as enabling fold-change detection, where the output depends on the fold change in the input signal rather than its absolute magnitude. These motifs regulate gene expression, integrate multiple signaling pathways, and modulate cellular responses to environmental cues, enabling cells to make adaptive, context-dependent decisions in processes like differentiation, apoptosis, and immune responses [1, 11, 12]. On the other hand, the NFBL motifs play a key role in regulating biological processes such as those involved in GPCR signaling [13–15], the lactose utilization network in E. coli [16, 17], the p53 tumor suppressor pathway [18], and cAMP signaling pathways [13, 19]. The NFBL motifs are essential for modulating the timing, level, and fluctuations of cellular responses, maintaining homeostasis, and ensuring the stability, precision, and adaptability of cellular functions in response to both internal and external stimuli. These motifs are integral to the overall efficiency and resilience of cellular systems [20–23].

Cellular regulatory mechanisms involving feed-forward loops, feedback loops, and autoregulatory processes have been extensively studied to enhance our understanding of cellular decision-making process [22, 24]. They are known to produce rich and complex dynamics, such as oscillations, multiple steady states, adaptation and both rapid and delayed responses [6, 23, 25–27]. However, the role and necessity of multiple regulatory network motifs in generating such dynamics remain not fully understood. Here, we explore the adaptive dynamics that emerge from the IFFL and NFBL network motifs, comparing them in terms of response time, return time, robustness, and their ability to generate maximal responses, to better understand how cells make selective decisions in response to changing environmental or intracellular signals.

The paper is organized as follows: Section 2 develops models for each network motif, deriving the sufficient conditions for adaptive responses and examining the steady-state behavior of each motif, including a discussion of their local stability. Section 3 compares the numerical predictions of the temporal behavior of each model in response to input signals with varying amplitude and persistence. The paper concludes with a discussion in Section 4.

Mathematical Models and Analysis

This section presents mathematical models for two biochemical network motifs that can generate adaptive dynamics, and derives the sufficient conditions for adaptation under persistent input signals. The first model represents a network with an incoherent feedforward loop (IFFL), shown on the left in Fig. 1, while the second model involves a negative feedback loop (NFBL) with autoregulation, depicted on the right in Fig. 1. Each network consists of three proteins: A, B, and C. It is well established that an IFFL network with fewer than three proteins cannot produce adaptive dynamics [28], whereas the NFBL motifs can [6, 29]. Here, protein A serves as the signal protein, whose abundance increases in response to the external input signal I. Protein B acts as an intermediate protein, interacting with protein C, the response protein.

In the IFFL model, the signal protein A positively interacts with both intermediate protein B and the response protein C, while the intermediate protein B negatively regulates the abundance of the response protein C. A well known biological example of an incoherent feedforward loop of this type is the NF-κB signaling circuit, where NF-κB activates the expression of both IL-8, a pro-inflammatory cytokine, and BCL3, a negative regulator that competes with NF-κB for binding to target promoters, including that of IL-8. This dual action results in a delay or inhibition of NF-κB-mediated IL-8 expression, illustrating the classic features of an incoherent feedforward loop [9]. Additional examples biological circuits involving IFFL motifs of this type can be found in [1, 24, 30], and references therein. On the other hand, in the NFBL model, the signal protein A positively interacts with the response protein C, and the response protein C positively regulates the abundance of the intermediate protein B while the intermediate protein negatively interacts with the response protein C, and positively promotes its own level. A good biological example of a negative feedback loop combined with a self-regulating positive feedback circuit is the *Bacillus subtilis* differentiation process into the competence state. In this system, differentiation

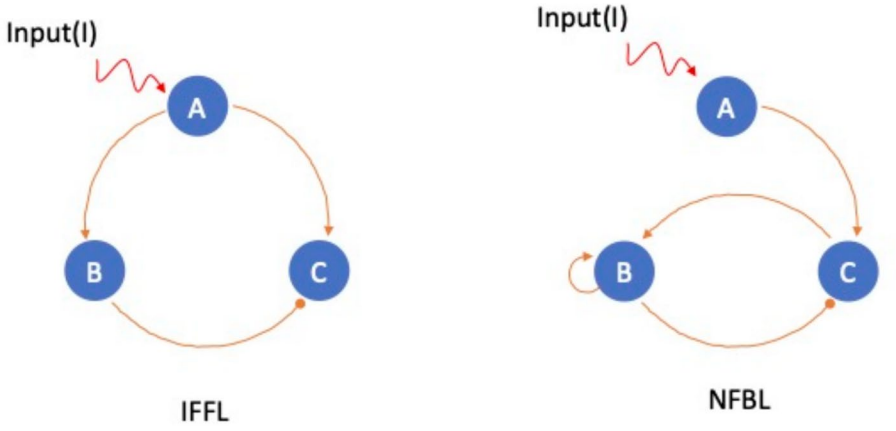

Fig. 1 A schematic representation of two network motifs involving three proteins that are capable of producing adaptive response dynamics to the prolonged input signal: Incoherent feedforward mechanism(IFFL) displayed on the left and negative feedback(NFBL) is shown on the right. Here, A is a signal protein, B is an intermediate protein and C is a response protein. In both interaction mechanisms, the input I activates only the signal protein A. The directed arrows represent a positive regulation while arrows with rounded ends represent the negative regulation

into competence is regulated by a negative feedback loop involving the transcription factor ComK and the activator protein ComS. ComK is necessary to trigger competence and also activates its own expression, creating a positive feedback loop [31, 32]. However, exit from the competence state is regulated by a negative feedback loop in which ComK indirectly represses the expression of its activator protein, ComS [33–35]. Additional examples of both real and synthetic biological circuits involving NFBL motifs can be found in [10, 36, 37], and references therein.

The IFFL Model

The model equations for the IFFL motif are given by Eqs. (1)–(3) [28]. Eq. (1) describes the dynamics of the signal protein A, where $v_A f(I)$ represent the gain rate and the second term models the degradation of this protein with a parameter β_A determining the half-life of this protein.

$$\frac{dA}{dt} = v_A f(I) - \frac{A}{\beta_A} \tag{1}$$

$$\frac{dB}{dt} = v_B \frac{A}{A + K_{AB}} - \frac{B}{\beta_B} \tag{2}$$

$$\frac{dC}{dt} = v_C \frac{A}{A + K_{AC}} \frac{K_{BC}}{B + K_{BC}} - \frac{C}{\beta_C} \tag{3}$$

Eq. (2) describes the dynamics of the intermediate protein B, in which the first term represents the gain rate of B due to A, and it is assumed to be Michaelis Menten type with the parameters of v_B and K_{AB} representing the maximum gain rate and the level of A required to reach the half of the maximum rate, respectively. Similar to the first equation, the second term represents the degradation of B and the parameter β_B determines this rate. Finally, the dynamics of the response protein C is given by Eq. 3). Here, the gain rate for C is the product of two terms. The first term $\frac{A}{A+K_{AC}}$ models the positive regulation of C by A, which is again assumed to be Michaelis Menten type with a parameter K_{AC}. The second term in this product ($\frac{K_{BC}}{B+K_{BC}}$) models the negative regulation of C by B, and K_{BC} is the Michaelis Menten parameter determining the level of protein B at which the inhibition happens at the half of its maximum rate. Here v_C represents the maximal gain rate for C. The last term in this equation models the degradation of this protein with a parameter β_C.

Steady State Analysis and Adaptation Conditions

To better understand the model dynamics as the model parameters vary, it is often helpful to express the model in dimensionless form and reduce the number of parameters without sacrificing its dynamic behavior. The details of nondimensionalization process are provided in the appendix. The dimensionless form of this model is

$$\begin{aligned}\frac{da}{d\tau} &= \alpha_0 - a \\ \frac{db}{d\tau} &= \frac{\alpha_1 a}{a+\alpha_2} - b \\ \frac{dc}{d\tau} &= \frac{a}{a+1}\frac{1}{b+1} - c\end{aligned}$$

where τ is a dimensionless time, and a, b and c are dimensionless variables for the proteins A, B and C, respectively. The degradation rates in a dynamical system directly influence several key aspects of its behavior, including stability, response time, return time, and adaptability [24]. For simplicity, we set $\beta_0 = \beta_1 = 1$ and assumed that all three proteins have the same degradation rates [1]. This reduces the number of parameters in the dimensionless model to three, namely α_0, α_1 and α_2. The adaptation requires the steady state level of c be independent of a and its parameters. When the conditions (i) $a^* \ll \alpha_2$, (ii) $a^* \ll 1$, (iii) $b^* \gg 1$ hold simultaneously, the dimensionless model further simplifies to

$$\frac{da}{dt} = \alpha_0 - a \tag{4}$$

$$\frac{db}{dt} = \frac{\alpha_1 a}{\alpha_2} - b \tag{5}$$

$$\frac{dc}{dt} = \frac{a}{b} - c \tag{6}$$

Adaptation in this model require a low affinity of signal protein A for the intermediate protein B compared to the response protein C. The steady state(a^*, b^*, c^*) of this model is

$$(a^*, b^*, c^*) = (\alpha_0, \frac{\alpha_0\alpha_1}{\alpha_2}, \frac{\alpha_2}{\alpha_1})$$

Note that in the adaptive regime, the steady state c^* is independent of a and its parameters; it is solely determined by the parameters of b. Furthermore, for the adaptation to occur in this model, b^* must have a linear dependency on the gain rate of a, which is α_0, with a slope of $\frac{\alpha_1}{\alpha_2}$ from Eq. (5) as depicted in Fig. 2. Moreover, b^* is defined for all α_0 values. To obtain a set of parameter values that leads to adaptive dynamics, a new parameter $s \gg 1$ is introduced, which allows us to further simplify the adaptation conditions to: (i) $\alpha_0 = s^{-1}$, (ii) $\alpha_1 = s^2$ and (iii) $\alpha_2 = 1$ and reduces the number of model parameters to one, namely s . However, this selection of parameters represents one of the many parameter sets that produces adaptive dynamics. More specifically, as an example, setting $s = 10^2$ uniquely determines the parameter values as $\alpha_0 = 10^{-2}, \alpha_2 = 1, \alpha_1 = 10^4$. Therefore, the adaptive model simplifies to

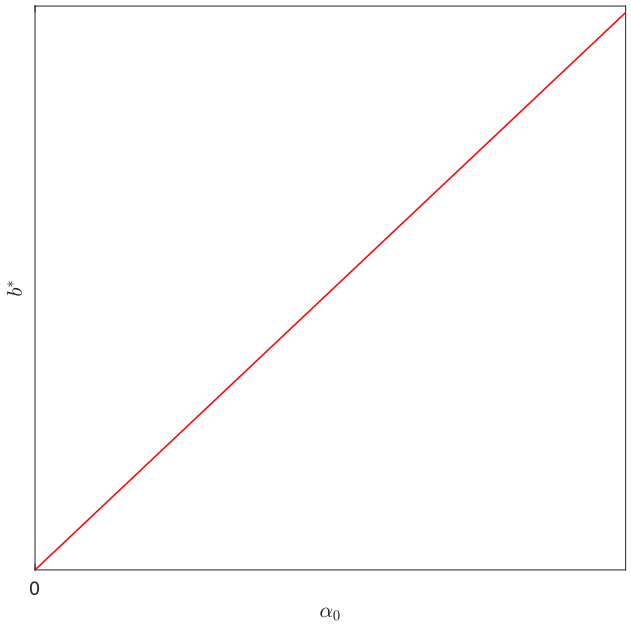

Fig. 2 Graphical demonstration of the steady state analysis of the IFFL model in the adaptive regime. The steady state of b increases linearly as a function of α_0, with a slope of $\frac{\alpha_1}{\alpha_2}$ for all values of α_0

$$\begin{aligned}\frac{da}{d\tau} &= s^{-1} - a \\ \frac{db}{d\tau} &= s^2 a - b \\ \frac{dc}{d\tau} &= \frac{a}{b} - c\end{aligned}$$

and its steady state in terms of s becomes

$$(a^*, b^*, c^*) = (s^{-1}, s, s^{-2}) \tag{7}$$

Since $s \gg 1$, the steady state of b is much larger than the steady state of a, which is also much larger than the steady state of c; namely, $c^* < a^* < b^*$ must hold. Note that the steady states of a and c are both less than one while the steady state of b is greater than one.

Local Stability Analysis

To study the local dynamics of this model in response to an increase in the input signal while it is at its resting state in the adaptive regime, the model equations are linearized around the steady state when $\alpha_0 = s^{-1}, \alpha_1 = s^2$ and $\alpha_2 = 1$(see appendix for the details). The linear model describing the dynamics of the deviation of each variable from its respective steady state becomes

$$\begin{aligned}\frac{d\Delta a}{d\tau} =& -\Delta a + \gamma \\ \frac{d\Delta b}{d\tau} =& s^2\Delta a - \Delta b \\ \frac{d\Delta c}{d\tau} =& s^{-1}\Delta a - s^{-3}\Delta b - c\end{aligned}$$

Here γ is a new input parameter representing an activatory input signal introduced in terms of the percentage of the basal gain rate of a when the system is at a resting state of $(\Delta a^*, \Delta b^*, \Delta c^*) = (0, 0, 0)$. The analytical solution of this system of differential equations [38] for the initial condition $\Delta a(0) = \Delta c(0) = \Delta c(0) = 0$ in terms of the parameters γ and s becomes

$$\Delta a(\tau) = \gamma\left(1 - e^{-\tau}\right) \tag{8}$$

$$\Delta b(\tau) = \gamma s^2\left(1 - (1+\tau)e^{-\tau}\right) \tag{9}$$

$$\Delta c(\tau) = \frac{\gamma\tau^2 e^{-\tau}}{2s} \tag{10}$$

After differentiating Eq. (10) with respect to τ and setting it equal to zero, one can compute that the maximum level of c as $\Delta c_{max} = 2\gamma s^{-1}e^{-2}$ attained at $\tau = 2$. For the values of $s = 1000$ and $\gamma = 1.2 \times \alpha_0$, the percentage increase in c relative to its steady state in response to a 20% increase in the input signal can be calculated as $100 \times \frac{\Delta c_{max}}{c^*} = 5.41\%$. Eq. (10) also shows that the time required to reach maximum responses is independent of the model parameters while the maximum deviation from the steady state of c is directly proportional to the input signal γ, and inversely proportional to $s \gg 1$. Since the reciprocal of s determines the steady state of a, and there will be no response when s is infinitely large.

The NFBL Model

The model equations for the NFBL motif are given by Eqs. (11–13). Similar to the IFFL model, Eq. (11) describes the dynamics of the signal protein A, where $v_A f(I)$ represents the gain rate and the second term models the degradation of this protein, with the parameter β_A determining its stability.

$$\frac{dA}{dt} = v_A f(I) - \frac{A}{\beta_A} \tag{11}$$

$$\frac{dB}{dt} = v_B \frac{B}{B + K_{BB}} \frac{C}{C + K_{CB}} - \frac{B}{\beta_B} \tag{12}$$

$$\frac{dC}{dt} = v_C \frac{A}{A + K_{AC}} \frac{K_{BC}}{B + K_{BC}} - \frac{C}{\beta_C} \tag{13}$$

Eq. (12) describes the dynamics of the intermediate protein B, which is the product of two Michaelis-Menten functions. Here, the first term ($v_B \frac{B}{B+K_{BB}}$) represents the gain rate of B

due to positive self-regulation of this protein, which is assumed to be the Michaelis Menten type with the parameters of v_B and K_{BB} representing the maximum rate and the level of B required to reach half of the maximum, respectively. The second term($\frac{C}{C+K_{CB}}$) models the gain in B due to positive regulation by the response protein C. Here, the parameter K_{CB} represents abundance of C required to reach the half of the maximum gain rate. The last term in this equation represents the degradation of B, with the parameter β_B. Finally, the dynamics of the response protein C is given by Eq. (13). The gain term for C is the product of two terms. The term $\frac{A}{A+K_{AC}}$ represents the positive regulation of C by A, which is assumed to be Michaelis Menten type with parameter K_{AC}. The second term ($\frac{K_{BC}}{B+K_{BC}}$) models the negative regulation of C by B. Here v_C represents the maximal gain rate for C. Lastly, the final term in this equation models the degradation of C, with the parameter β_C determining its degradation rate.

Steady State Analysis and Adaptation Conditions

After scaling the time and state variables as described in the appendix, the dimensionless form of the model is given by

$$\begin{aligned}\frac{da}{d\tau} =&\alpha_0 - \beta_0 a\\ \frac{db}{d\tau} =&\alpha_1 \frac{b}{b+\alpha_3}\frac{c}{c+\alpha_4} - \beta_1 b\\ \frac{dc}{d\tau} =&\frac{a}{a+1}\frac{1}{b+1} - c\end{aligned}$$

Here again τ is the dimensionless time and a, b, c represent scaled levels of proteins A, B, C, respectively.

The adaptive dynamics requires the independence of the steady state of the response protein C from the signal protein A. Since B is not regulated by A in this model, one way to achieve the adaptive dynamics is to have positive regulation of B by itself [12]. Under the assumption of $\beta_0 = \beta_1 = 1$, if (i) $\alpha_4 \gg c^*$ and (ii) $\alpha_3 \gg b^*$ both hold simultaneously, the dimensionless model simplifies to

$$\frac{da}{d\tau} =\alpha_0 - a \tag{14}$$

$$\frac{db}{d\tau} = (\tilde{\alpha}_1 c - 1)\, b \tag{15}$$

$$\frac{dc}{d\tau} =\frac{a}{a+1}\frac{1}{b+1} - c \tag{16}$$

where $\tilde{\alpha}_1 = \frac{\alpha_1}{\alpha_3\alpha_4}$. Biologically speaking, the adaptive dynamics in the NFBL model requires a low affinity of the intermediate protein B for itself, as well as a low affinity of response protein C for the intermediate protein B. As seen in Eq. (15), $\frac{db}{d\tau}$ is directly proportional to b. When $\frac{da}{d\tau} = \frac{db}{d\tau} = \frac{dc}{d\tau} = 0$, this model produces the following two steady states. The first steady state is at

$$(a^*, b^*, c^*) = (\alpha_0, 0, \frac{\alpha_0}{\alpha_0 + 1})$$

and the second steady state is at

$$(a^*, b^*, c^*) = (\alpha_0, \frac{\alpha_0 \tilde{\alpha}_1}{\alpha_0 + 1} - 1, \frac{1}{\tilde{\alpha}_1}). \tag{17}$$

The second steady state is biologically meaningful only if $\frac{\alpha_0 \tilde{\alpha}_1}{\alpha_0 + 1} > 1$. Notice that the steady state of c in the the first steady solely depends on the abundance of signal protein determined by α_0. Therefore, the NFBL model cannot display adaptive dynamics at this steady state, and the adaptation can only occur when the model attains the second steady state. Fig. 3 shows a graphical representation of how the steady state of b changes as a function of the gain rate α_0 in the adaptive regime for this model. As seen in this plot, the steady state level of b is a nonlinear saturating function of α_0, and this dependence is a Michaelis Menten type with a maximum value of $\tilde{\alpha_1} - 1$. For adaptation to occur, $b^* > 0$ must hold, leading to $\alpha_0 > \alpha_0^{critical} = \frac{1}{\tilde{\alpha}_1 - 1}$. Unlike the IFFL model, in the NFBL model, for b^* to be biologically meaningful in the adaptive regime, α_0 must exceed a critical value $\alpha_0 > \alpha_0^{critical}$.

From Eq. (16), $c^* < 1$ always holds. At the steady state, given by Eq. (17), the first adaptation condition $c^* = \frac{\alpha_3 \alpha_4}{\alpha_1} \ll \alpha_4$ simplifies to $\alpha_1 \gg \alpha_3$. To obtain a set of parameter values for the adaptive dynamics, we can choose $\alpha_4 = 1$, which results in $c^* = \frac{\alpha_3}{\alpha_1} \ll 1$, ensuring that the first condition is always satisfied. Introducing a large value $s \gg 1$ further simplifies the two adaptation conditions to

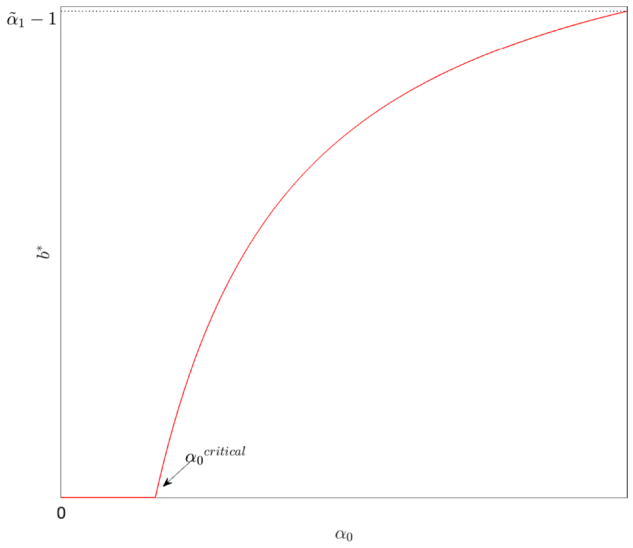

Fig. 3 A graphical representation of the steady state analysis of the NFBL model in the adaptive regime. The steady state of b as a function of α_0 is a nonlinear saturating function with a maximum value of $\tilde{\alpha_1} - 1$ (see the text for the details)

$$\alpha_3 = s\left(\frac{s\alpha_0}{\alpha_0+1}-1\right) = \frac{s^2\alpha_0}{\alpha_0+1} > 0$$
$$\alpha_1 = s^2\left(\frac{s\alpha_0}{\alpha_0+1}-1\right) = s^3\frac{\alpha_0}{\alpha_0+1} > 0$$

Using these estimates, the adaptive NFBL model becomes

$$\begin{aligned}\frac{da}{d\tau} &= \alpha_0 - a\\ \frac{db}{d\tau} &= (sc-1)b\\ \frac{dc}{d\tau} &= \frac{a}{a+1}\frac{1}{b+1} - c\end{aligned}$$

and its steady state becomes

$$(a^*, b^*, c^*) = (\alpha_0, \frac{\alpha_0 s}{\alpha_0+1} - 1, s^{-1}) \tag{18}$$

Since α_0 is the steady state of *a* and *a* positively regulates *c*, we restrict $\frac{1}{9} \leq \alpha_0 \leq 9$, which covers the range from 10% to 90% of the maximal gain rate of *c* as detailed in the simulation section. Therefore, in the adaptive regime, the steady state of *b* is significantly larger than the steady states of both *a* and *c*, and the steady state of *b* is greater than one, while the steady state of *c* is much smaller than one.

Local Stability Analysis

To investigate local dynamics of the NFBL model, it is studied analytically by linearizing the model equations in the vicinity of the steady state given by Eq. 18) as detailed in the appendix. For the half maximal gain rate of *c* due to *a*, if we set $\alpha_0 = 1$, then α_1 and α_3 become $\frac{s^3}{2}$ and $\frac{s^2}{2}$ respectively, simplifying the model equations to

$$\begin{aligned}\frac{d\Delta a}{d\tau} &= -\Delta a + \gamma\\ \frac{d\Delta b}{d\tau} &= (\frac{s^2}{2} - s)\Delta c\\ \frac{d\Delta c}{d\tau} &= \frac{1}{2s}\Delta a - \frac{2}{s^2}\Delta b - \Delta c\end{aligned}$$

where γ is a newly introduced input signal that represents the input when the model is at the resting state of $(\Delta a^*, \Delta b^*, \Delta c^*) = (0, 0, 0)$. This model can be solved analytically [38] to get the solution for the initial condition $\Delta a(0) = \Delta c(0) = \Delta c(0) = 0$ in terms of γ and $s \gg 1$ as

$$\Delta a(\tau) = \gamma\left(1 - e^{-\tau}\right) \tag{19}$$

$$\Delta b(\tau) = \gamma s \left[\frac{1}{4}(1 - e^{-\tau}) - \frac{\sqrt{3}}{6} e^{-\frac{\tau}{2}} \sin(\frac{\sqrt{3}}{2}\tau) \right] \tag{20}$$

$$\Delta c(\tau) = \frac{\gamma}{2s} \left[\left(\frac{\sqrt{3}}{3} \sin(\frac{\sqrt{3}}{2}\tau) - \cos(\frac{\sqrt{3}}{2}\tau) \right) e^{-\frac{\tau}{2}} + e^{-\tau} \right] \tag{21}$$

Notice that the solution is oscillatory in the adaptive regime. From Eq. (21), one can calculate the percentage maximum value of c relative to its basal level as $100 \times \frac{|\Delta c_{max}|}{c_1^*} = 4.04\%$, which occurs at $\tau_{rs} = 2.055$ when $\alpha_0 = 1$. At $\alpha_0 = 1/9$ and 9, these values become $100 \times \frac{|\Delta c_{max}|}{c_1^*} = 7.28\%$ and 0.81% attained at $\tau_{rs} = 2.054$ and 2.054, respectively. The local stability analysis of this model shows that the maximum deviation from the steady state of c is directly proportional to the input signal γ, and it is inversely proportional to $s \gg 1$. Moreover, the time required to reach the peak is determined by two exponential functions and two trigonometric functions. Like in the IFFL model, the reciprocal of s measures the steady state of a, and if there is no signaling protein there will be no response as expected.

Numerical Simulations and Response Dynamics

One way to compare the dynamics of the IFFL and NFBL models is to examine the responses they generate as the input signal varies. In this section, we numerically simulate the model equations in Matlab utilizing its ode15s solver. For all simulations, the parameter s held constant at $s = 5000$ while the amplitude and persistency of the input signal are varied.

Prolonged Input Signals and Response Dynamics

We first examine how each model responds to a prolonged signal with increasing amplitude. Four metrics are used to quantify the response dynamics. Each metric captures a different aspect of the response curve. The first metric is the *response time*(τ_{rs}), which quantifies the time required to reach the maximum level of c, namely $c(\tau_{rs}) = c_{max}$. The second metric is the *return time* (τ_{rt}), which measures the time required for the response level to return within 5% range of its pre-steady state, defined as the resting state of the protein prior to the signal. c_{rt} satisfies the condition $\left| \frac{c(\tau_{rt}) - c_1^*}{c_1^*} \right| \times 100 \leq 5$, where c_1^* is the steady state level of c before the signal. The third metric is the *maximum percentage increase* (c_{max}) in c relative to the pre-steady state level, which is given by $c_{max} = \left| \frac{c(\tau_{rs}) - c_1^*}{c_1^*} \right| \times 100$. Again here, c_1^* represents the steady state of c before the signal. The fourth metric is the *percentage adaptation error* (a_{error}), which measures the level of adaptation after applications of the signals, which can be calculated by using the formula $a_{error} = \left| \frac{c_2^* - c_1^*}{c_1^*} \right| \times 100$, where c_1^* represents the steady state of c before the signal, and c_2^* represents the steady state of c after the signal. We assume that the models exhibit perfect adaptation if this metric is less than 0.04%. Referring to Eqs. (14)–(16), since α_0 is the sole parameter determining the steady state of a, which positively regulates c, we restrict $\frac{1}{9} \leq \alpha_0 \leq 9$. This range implies that a can influence the gain rate of c by between 10% and 90% of its maximum value. Since the

gain rate of c due to a follows a Michaelis-Menten type function, both excessively small and large values of α_0 outside of this range result in a negligible change in the gain rate of c. For example, for a fixed value of b, $\alpha_0 = 1/9, 1$ and 9 result in gain rates of 90%, 50% and 10% of maximal gain rate of c due to a, respectively.

Our simulation results, depicting the response dynamics as the input signal changes for both models, are shown in Fig. 4. To capture a wide range of changes in the input signal amplitude, the x-axis is scaled logarithmically in these simulations. As seen in Fig. 4A), the response metric τ_{rs} decreases as the input amplitude increases in both models. τ_{rs} reaches its lowest value for the highest input amplitude, while it is the highest ($\tau_{rs} \approx 2$) when the input signal amplitude is the lowest, corresponding to a 1% increase in its basal level.

The simulation curve for τ_{rs} in the IFFL model(red curve) and the NFBL model with $\alpha_0 = 1/9$(blue dash curve) are comparable up to a 200-fold increase in the input signal amplitude. However, between 200 and 1000 fold change in the amplitude, τ_{rs} for the IFFL model continues to decrease, reaching 0.5 at a 1000-fold increase. In contrast, for the NFBL model, τ_{rs} seems to saturate around 0.63.

For all levels of input signal amplitude, τ_{rs} is always shorter in the IFFL model compared to the NFBL model when $\alpha_0 = 1$ or 9(black and cyan dashed curves). As the signal

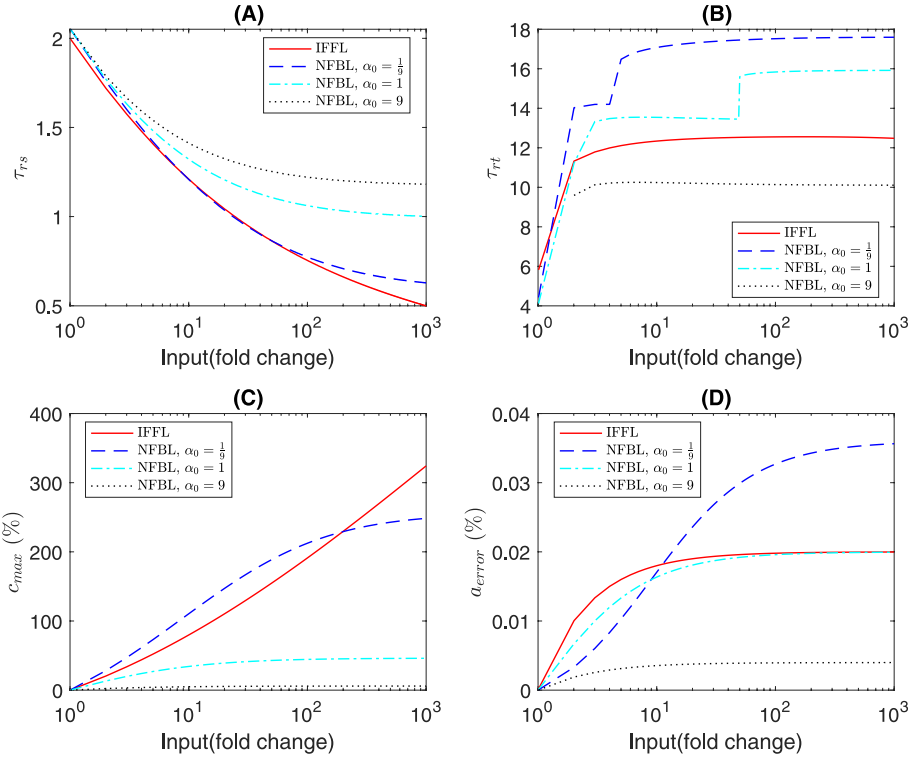

Fig. 4 Response metrics for the IFFL and NFBL models as the amplitude of the input signal increases. Four metrics are depicted in this simulation: **(A)** response time (τ_{rs}), **(B)** return time (τ_{rt}), **(C)** maximum response (c_{max}), and **(D)** adaptation error (a_{error}). These metrics are calculated using 1000 evenly spaced values for the input signal amplitudes, ranging from 1.1 to 1000, corresponding to a 1% to 1000-fold increase in input signal amplitude. Note that the x-axis is on a logarithmic scale to capture a wide range of input signal amplitudes

amplitude increases, the difference in τ_{rs} between the IFFL and NFBL models becomes more pronounced, indicating that the NFBL model responds slower to stronger input signals compared to the IFFL model.

This simulation also shows that the response time can be regulated in the NFBL model, but not in the IFFL model when all three proteins have the same degradation rates for the fixed input signal amplitude. Unless protein A has a very high affinity for C in the NFBL model, τ_{rs} in the IFFL model is always shorter. When A has a high affinity for C, the models have comparable τ_{rs} values for input signals with amplitudes less than a 200-fold increase. For signals with amplitudes greater than 200-fold, the response time remains shorter in the IFFL model.

Fig. 4B displays the simulation result for τ_{rt} metric. The return time τ_{rt} increases as the amplitude of the input signal increases and reaches some maximal values in both models. The stronger the signal is, the longer it takes for the models to return to their respective pre-steady state levels. This metric takes its values between 4 and 18 unit of dimensionless time as the input increases from 1% to 1000 fold increase in the amplitude of the signal. Compared to the IFFL model(red solid line), τ_{rt} takes larger value in the NFBL model for the parameter values of $\alpha_0 = 1/9$ and $\alpha_0 = 1$(blue dotted curve and cyan dashed curve), and smaller value for the parameter value of $\alpha_0 = 9$(black dotted curve). Our simulation shows a maximum of two fold increase in the return time in the IFFL model as the signal amplitude increases, but this increase in the NFBL model is 4-5 fold when $\alpha_0 = 1/9 \text{ and } 1$, and it is about 2.5 fold when $\alpha_0 = 9$. This is due to the fact that for the larger value of this parameter, the maximum response level in the NFBL model is much smaller. The sharp jumps in this metric for the NFBL model when $\alpha_0 = 1/9 \text{ and } 1$ are due to the oscillatory nature of the dynamics produced by this model. Our simulations depict that it takes longer for the NFBL model to return to the pre-steady state compared to the IFFL model unless A has a low affinity to C in the NFBL model producing much smaller maximal response.

Fig. 4C displays the simulation result for the maximum response metric c_{max}, which increases as the input signal amplitude increases in both models. c_{max} attains its lowest value for the weakest signal while it takes its highest value around 320%(red curve) when the input signal is the strongest for the IFFL model, this value is about 250%(blue dashed curve) for the NFBL model that occurs when $\alpha_0 = 1/9$. Our simulation predicts that c_{max} increases as the input increases in the IFFL model, but it saturates around 250%(blue dashed curve), 45%(cyan dashed curve) and 6%(black dotted curve) in the NFBL models when $\alpha_0 = 1/9, 1 \text{ or } 9$, respectively. The NFBL model with $\alpha_0 = 1/9$ produces the highest response until about 210 fold change in the amplitude of the signal, and this response starts saturating for the stronger signals, and levels off around 250%. The difference in the percentage maximal changes in the response compared to the respective pre-steady state levels between the NFBL and IFFL models can be as much as 60 fold. The IFFL model produces higher response compared to the NFBL model for strong signals, while the NFBL with $\alpha_0 = 9$ produces a maximal response of 6% even for the strongest input signal.

Fig. 4D displays the simulation result for a_{error} metric. The adaptation error a_{error} increases as the input increases, but in all simulations it stays below 0.04%, indicating almost perfect adaptation attained by the models, which also shows that adaptability of the models are robust against up to 1000-fold increase in the amplitude of the input signal.

This simulation shows that the IFFL model responds to the strong input signal faster, and produces higher response levels and returns back to its pre-steady state sooner compared

to the NFBL, the only exception is the NFBL model with $\alpha_0 = 9$, which returns back to its pre-steady state sooner, but its capacity of producing responses to the signal is small (Fig. 4B and C).

Pulse Type Repetitive Input Signals and Response Dynamics

To further investigate and compare the dynamics produced by the IFFL and NFBL models, we simulated both models using pulse-type repetitive input signals with varying amplitude and persistency, while the models are at their respective steady states. The simulation results are shown in Fig. 5A--D. In each simulation, the NFBL model was run for two different values of $\alpha_0 = 1/9$ and $\alpha_0 = 1$, since the model does not produce a strong enough response when $\alpha_0 = 9$ (see Fig. 4C). In all simulations, the red solid curve represents the IFFL model response, while the blue dotted and blue dash-dotted curves represent the NFBL model responses with $\alpha_0 = 1/9$ and $\alpha_0 = 1$, respectively. These two values of α_0 in the NFBL model correspond to high and moderate affinity levels of the signaling protein A to the response protein C. In each plot, the signal profile is shown at the top, and the response protein dynamics are shown at the bottom.

Response dynamics to weak-short input signals: We simulated the IFFL model and NFBL model dynamics in response to weak-short input signals, and the result is shown in Fig. 5A. For this simulation, a signal with an amplitude of $\alpha_0 = 2$ and persistency of 1 for every 10 unit of time is applied to both models four times. The x-axis is the dimensionless time τ and y-axis is the percentage changes in the response relative to their respective steady states prior to the signal. To produce this simulation, when the models are at their respective resting state at $\tau = 0$, the signal is turned on by setting $\alpha_0 = 2$ until $\tau = 1$, at this time point it is tuned off by resetting α_0 back to its baseline value of 1, and waited until $\tau = 10$ so that the models converge back to their resting state. Our simulations predict that waiting 10 units of time is sufficiently long for the models to converge back to their resting states before the next signal. At $\tau = 10$, the signal is turned on for a unit of time again and turned off at $\tau = 11$. This pattern of turning the signal on for one unit of time for every 10 unit of time is continued until $\tau = 40$.

As seen in this simulation, the dynamics are all oscillatory for both models due to the nature of the signals applied; however, the NFBL model produces higher oscillatory responses compared to the IFFL model when $\alpha_0 = 1/9$, but not when $\alpha_0 = 1$. This pattern of dynamics is consistent for each signal application. The maximum response to the first signal for the NFBL with $\alpha_0 = 1/9$ is 122.5%, attained at $\tau = 1.26$, whereas this value is 117% at $\tau = 1.17$ for the IFFL model. The NFBL model with $\alpha_0 = 1$ reaches a maximum of 110.8% at $\tau = 1.31$ for the first signal. The repeated response pattern is not surprising as all the models assume adaptive dynamics for the selected parameter values. After turning off the signal, waiting 9 units of time is long enough for the models to settle back down to their respective steady states, and all the models produces similar dynamics for the successive signal applications.

Response dynamics to pulse type very strong short input signals: The dynamics produced by the IFFL and NFBL models were simulated in response to a strong, short-pulse input signal with an amplitude of $\alpha = 400$ and a duration of 1 time unit for every 4 units of time. The simulation results are shown in Fig. 5B. To generate this simulation, the signal was activated at $\tau = 0$ by setting $\alpha = 400$ and remained on until $\tau = 1$, then it was turned

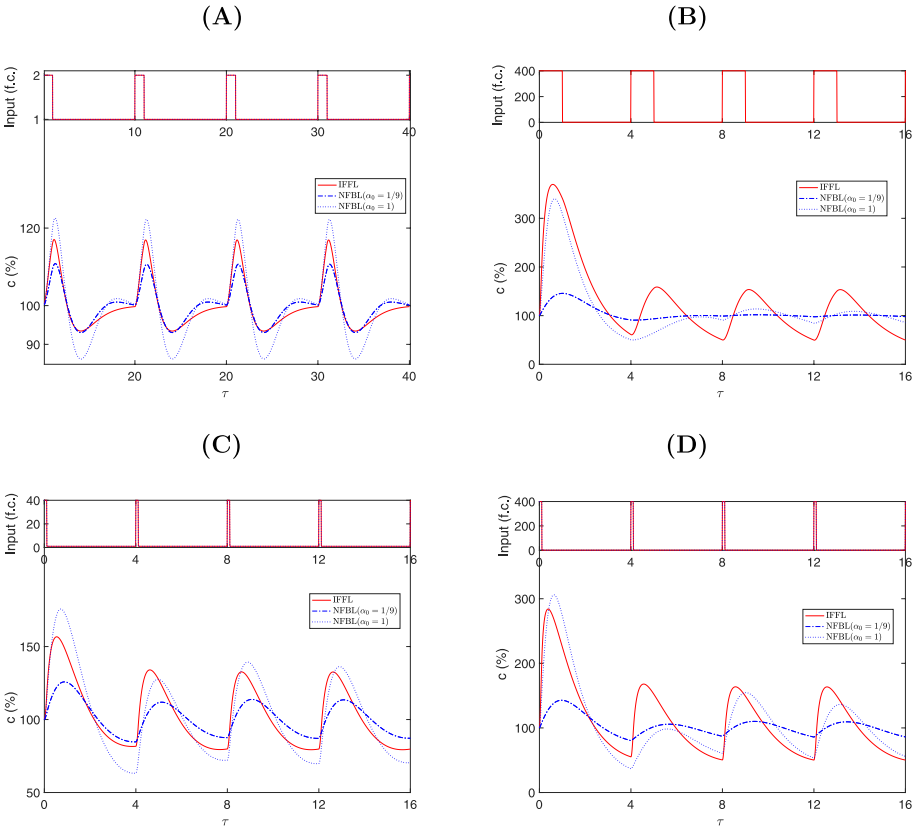

Fig. 5 Dynamic responses of the IFFL and NFBL models in response to repetitive pulse type signals with varying amplitude and persistency. (**A**) Response dynamics for the signal with an amplitude of $\alpha_0 = 2$ and a persistency of one for every 10 unit of time. (**B**) Response dynamics for the signal with an amplitude of $\alpha_0 = 400$ and a persistency of one for every 10 unit of time, (**C**) Response dynamics for the signal with an amplitude of $\alpha_0 = 40$ and a persistency of 1/10 for every 10 unit of time, (**D**) Response dynamics for the signal with an amplitude of $\alpha_0 = 400$ and a persistency of 1/10 for every 10 unit of time. The top plot shows the signal profile and the bottom plot shows the response dynamics for the IFFL model(red solid curve), the NFBL model with $\alpha_0 = 1/9$ (blue dotted curve), and finally the NFBL model with $\alpha_0 = 1$(blue dash-dotted curve). These two values of α_0 mimic high and moderate affinity of signal protein A to the response protein C

off at $\tau = 1$ by resetting $\alpha_0 = 1$. The signal stayed off until $\tau = 4$, after which it was turned on again for one unit of time and turned off at $\tau = 5$. This on-off pattern was repeated four times until $\tau = 16$.

This simulation shows that the NFBL model with $\alpha_0 = 1/9$ produces slightly smaller oscillatory responses ($\sim$340%) attained at $\tau = 0.64$, compared to the IFFL model ($\sim$364%) attained at $\tau = 0.57$ for the first signal. However, surprisingly, the response of the NFBL model diminishes significantly in later times (after the 4th signal application), dropping to $\sim$108%, while the IFFL model produces a $\sim$154% response to the same signal profile. On the other hand, the NFBL model with $\alpha_0 = 1$ produces small oscillatory responses ($\sim$ 145%) attained at $\tau = 0.98$, compared to the IFFL model's $\sim$364% at $\tau = 0.57$ after the first input signal. The response in the NFBL model with $\alpha_0 = 1$ diminishes completely in

later times (∼101.3%), and the model becomes almost unresponsive to the input signal. Our simulations suggest that this is due to the inhibitory effect of the intermediate protein *B* on the response protein *C*, which is significantly larger than the activatory effect of the signal protein *A* on the same protein for this type of input signal profile.

Response dynamics to pulse type strong-brief signals: We also simulated the dynamics produced by the IFFL and NFBL models in response to a brief, very strong input signal. The signal had an amplitude of $\alpha_0 = 40$ and a persistency of 1/10 for every 4 units of time. The simulation result is depicted in Fig. 5C. To produce this simulation, the signal is briefly turned on at $\tau = 0$ and remains on until $\tau = 0.1$, at which point it is turned off by resetting α_0 back to its basal level of 1. The signal is left off until $\tau = 4$. At $\tau = 4$, the signal is turned on again for 0.1 units of time and turned off at $\tau = 4.1$. This pattern is repeated four times until $\tau = 16$.

This simulation shows that the NFBL model with $\alpha_0 = 1/9$ produces higher oscillatory responses (∼174%) attained at $\tau = 0.71$, compared to the IFFL model (∼156%) at $\tau = 0.52$ after the first signal. The response diminishes in later times, and becomes comparable to the response produced by the IFFL model. After the application of the 4th signal, the response produced by the IFFL model is ∼132%, while it is ∼136% for the NFBL model with $\alpha_0 = 1/9$. On the other hand, the NFBL model with $\alpha_0 = 1$ produces a response with smaller amplitude (∼125%) attained at $\tau = 0.86$ for the first signal, and the responses for successive signals become significantly smaller (∼113%). This is again due to the inhibitory effect of the intermediate protein *B* on the response protein *C*, which dominates the activatory effect of the signal protein *A* on *C*.

Response dynamics to pulse type very strong-brief signal: The dynamics produced by the IFFL and NFBL models were also simulated in response to a brief, very strong input signal. The signal had an amplitude of $\alpha_0 = 400$ and a persistency of 1/10 for every 4 units of time. The simulation result is depicted in Fig. 5D. To produce this simulation, the signal is briefly turned on at $\tau = 0$ and remains on until $\tau = 0.1$, at which point it is turned off by resetting $\alpha_0 = 1$. The signal is then left off until $\tau = 4$. At $\tau = 4$, the signal is turned on again for 0.1 units of time and turned off at $\tau = 4.1$ repeating this pattern 4 times until $\tau = 16$.

This simulation shows that the NFBL model with $\alpha_0 = 1/9$ produces higher oscillatory responses (∼302%) attained at $\tau = 0.65$, compared to the IFFL model (∼280%) at $\tau = 0.41$ after the first signal. However, in later times, the response diminishes significantly and becomes smaller in amplitude than the response produced by the IFFL model. After the 4th signal, the response for the NFBL model is ∼135%, while for the IFFL model it is ∼163%. On the other hand, the NFBL model with $\alpha_0 = 1$ produces a response with smaller amplitude (∼142%) attained at $\tau = 0.91$ for the first signal, and the responses for successive signals become significantly smaller (∼109%) due to the inhibitory effect of the intermediate protein *B* on the response protein *C*. It is surprising to see that the NFBL model with $\alpha_0 = 1/9$ produces a significantly smaller response compared to the IFFL model after the first signal.

Conclusion and discussion

We studied two well-known network motifs capable of generating adaptive dynamics in response to prolonged input signals. For each motif, we identified the sufficient conditions for adaptation and compared the resulting dynamics. Both mechanisms involve three proteins, which is the minimum number required for adaptive responses in the IFFL motif, but not necessarily for the NFBL motif [28].

Our mathematical analysis showed that the adaptive dynamics in the IFFL motif are more robust with larger parameters ranges compared to those in the NFBL motif. In the adaptive regime, our analysis reveals that the steady-state level of the intermediate protein increases linearly as the steady-state level of the signal protein rises in the IFFL model, while this relation is saturating for the NFBL model and the steady-state of the signal protein must exceed a certain threshold, which has been reported in an earlier experimental study [39]. They studied the chemotactic responses of bacteria and amoeba to input signals and observed that bacteria employing the NFBL failed to exhibit adaptation [40, 41], whereas amoeba utilizing the IFFL showed adaptation to the input signal [42]. The saturating relationship between input signal and response protein levels in the NFBL model has recently been observed in a genetically engineered circuit [36]. In this study, they designed a robust perfect adaptation circuit that involves a two-node negative feedback loop coupled with linear positive feedback, and experimentally measured the relationship between the steady-state levels of the monomeric transcriptional activator and input signals across various promoter mutants. they observed that this relationship indeed saturates in all mutants.

The local stability analysis of both models reveals distinct behaviors. In the IFFL model, the response time is exactly twice the protein degradation rate and is independent of the signal amplitude. In contrast, the response time in the NFBL model slightly larger than twice the degradation rate. For both models, the maximum response level is proportional to the input signal amplitude. However, while the dynamics near steady state are exponential in the IFFL model, they are oscillatory in the NFBL model. Both IFFL and NFBL motifs reduce response time [1, 20], our local analysis shows that the response times for both models are comparable, each being approximately twice the protein degradation rate, which agrees well with the measurements reported in an experimental study for a negative feedback system [36]. These consistencies suggest that the IFFL motif may be particularly effective in environments where stable and predictable responses are necessary. On the other hand, the NFBL motif showed slightly more variability in response time, varying around twice the degradation rate. The NFBL model also demonstrated oscillatory behavior near steady state, in contrast to the exponential dynamics observed in the IFFL motif. These oscillations may offer a potential advantage in situations where more complex, time-varying responses are required, such as in processes involving periodic or transient signals. Despite these differences, both motifs exhibited a linear relationship between the signal amplitude and the maximum response, highlighting their common ability to scale their outputs according to the input. The richer dynamics of the NFBL motif, however, suggest that it could provide more flexible regulatory control, potentially enabling cells to fine-tune their responses based on environmental cues.

To conclude, our comparison underscores the importance of feedback architecture in shaping the temporal characteristics and flexibility of adaptive responses. The inherent complexity and nonlinearity of cellular networks empower cells to perform intricate and coordi-

nated functions. However, because of this complexity, examining individual components in isolation does not fully reveal how these networks function as a whole. To gain a comprehensive understanding of the dynamics and regulation of these networks, a systems-level approach is crucial. Our *in silico* experiments provide testable predictions that can inform future research aimed at enhancing our understanding of protein dynamics, regulation, and signal adaptation.

A. Appendix

This section provides the details of non-dimensionalization and local stability analysis of the IFFL and NFBL models.

A.1 Derivation of the dimensionless model for the IFFL motif

The IFFL model given by Eqs. (1)–(3) consists of a system of three nonlinear differential equations with 10 governing parameters. To obtain a dimensionless form, we first introduce dimensionless variables for time t and state variables A, B and C :

$$\tau = \frac{t}{\beta_C},\ a = \frac{A}{K_{AC}}, b = \frac{B}{K_{BC}} \text{ and } c = \frac{C}{v_C \beta_C} \tag{A1}$$

By differentiation, the corresponding relationships become

$$dt = d\tau \beta_C,\ dA = K_{AC} da, dB = K_{BC} db \text{ and } dC = v_C \beta_C dc \tag{A2}$$

After substituting these quantities into the model equations in Eqs. (1)–(3) and making necessary simplifications, we obtain the dimensionless form as

$$\begin{aligned}
\frac{da}{d\tau} &= \alpha_0 - \beta_0 a \\
\frac{db}{d\tau} &= \frac{\alpha_1 a}{a + \alpha_2} - \beta_1 b \\
\frac{dc}{d\tau} &= \frac{a}{a+1}\frac{1}{b+1} - c
\end{aligned}$$

where $\alpha_0 = \frac{\beta_C v_A f(I)}{K_{AC}}, \alpha_1 = \frac{\beta_C v_B}{K_{BC}}, \alpha_2 = \frac{K_{AB}}{KAC}, \beta_0 = \frac{\beta_C}{\beta_A}, \beta_1 = \frac{\beta_C}{\beta_B}$.

A.2 Linearization of the dimensionless IFFL model

The dimensionless IFFL model simplifies to the following equations in the adaptive regime under the assumptions outlined in Section 2.1

$$\begin{aligned}\frac{da}{dt} &= f_a(a,b,c) = \alpha_0 - a \\ \frac{db}{dt} &= f_b(a,b,c) = \frac{\alpha_1 a}{\alpha_2} - b \\ \frac{dc}{dt} &= f_c(a,b,c) = \frac{a}{b} - c\end{aligned}$$

The steady state(a^*, b^*, c^*) of this model can be calculated by setting $\frac{da}{d\tau} = \frac{db}{d\tau} = \frac{dc}{d\tau} = 0$, and solving the resulting system simultaneously for (a, b, c), which leads to

$$(a^*, b^*, c^*) = (\alpha_0, \frac{\alpha_0\alpha_1}{\alpha_2}, \frac{\alpha_2}{\alpha_1})$$

To obtain a linear model representing the local dynamics around this steady state, we compute the Jacobian matrix and evaluate it at the steady state, which results in

$$J^*(a^*, b^*, c^*) = \begin{pmatrix} \frac{\partial f_a}{\partial a} & \frac{\partial f_a}{\partial b} & \frac{\partial f_a}{\partial c} \\ \frac{\partial f_b}{\partial a} & \frac{\partial f_b}{\partial b} & \frac{\partial f_b}{\partial c} \\ \frac{\partial f_c}{\partial a} & \frac{\partial f_c}{\partial b} & \frac{\partial f_c}{\partial c} \end{pmatrix}_{(a^*,b^*,c^*)} = \begin{pmatrix} -1 & 0 & 0 \\ \frac{\alpha_1}{\alpha_2} & -1 & 0 \\ \frac{\alpha_2}{\alpha_0\alpha_1} & \frac{-\alpha_2^2}{\alpha_0\alpha_1^2} & -1 \end{pmatrix}$$

After defining new variables describing the deviations of each dimensionless variable from its steady state as $\Delta a = a - a^*$, $\Delta b = b - b^*$ and $\Delta c = c - c^*$, the linear model approximating the dynamics of the nonlinear model near the steady state becomes

$$\begin{aligned}\frac{d\Delta a}{dt} &= -\Delta a \\ \frac{d\Delta b}{dt} &= \gamma_0\Delta a - \Delta b \\ \frac{d\Delta c}{dt} &= \gamma_1\Delta a + \gamma_2\Delta b - \Delta c\end{aligned}$$

where $\gamma_0 = \frac{\alpha_1}{\alpha_2} > 0$ and $\gamma_1 = \frac{\alpha_2}{\alpha_0\alpha_1} > 0$ and $\gamma_2 = \frac{-\alpha_2^2}{\alpha_0\alpha_1^2} < 0$. This model can be solved analytically to study the local dynamics in the vicinity of the steady state.

A.3 Derivation of the dimensionless model for the NFBL motif

The NFBL model, as given by Eqs. (11)–(13), consists of a system of three nonlinear differential equations and eleven parameters. To obtain a dimensionless form, we can use the same definitions for the dimensionless variables and time as provided in Eq. (A.1) and Eq. (A.2). After substituting Eq. (A.2) into the model equations and performing the necessary simplifications, the dimensionless form of the model becomes

$$\begin{aligned}\frac{da}{d\tau} =&\alpha_0 - \beta_0 a\\ \frac{db}{d\tau} =&\alpha_1 \frac{b}{b+\alpha_3}\frac{c}{c+\alpha_4} - \beta_1 b\\ \frac{dc}{d\tau} =&\frac{a}{a+1}\frac{1}{b+1} - c\end{aligned}$$

where $\alpha_0 = \frac{\beta_C v_A f(I)}{K_{AC}}, \alpha_1 = \frac{\beta_C v_B}{K_{BC}}, \alpha_3 = \frac{K_{BB}}{K_{BC}}, \alpha_4 = \frac{K_{CB}}{v_C \beta_C}, \beta_0 = \frac{\beta_C}{\beta_A}$ and $\beta_1 = \frac{\beta_C}{\beta_B}$.

A.4 Linearization of the dimensionless NFBL model

The dimensionless NFBL model simplifies to the following equations in the adaptive regime under the assumptions outlined in Section 2.2

$$\begin{aligned}\frac{da}{d\tau} =&g_a(a,b,c) = \alpha_0 - a\\ \frac{db}{d\tau} =&g_b(a,b,c) = (\tilde{\alpha}_1 c - 1)\, b\\ \frac{dc}{d\tau} =&g_c(a,b,c) = \frac{a}{a+1}\frac{1}{b+1} - c\end{aligned}$$

where $\tilde{\alpha}_1 = \frac{\alpha_1}{\alpha_3 \alpha_4}$. The steady states$(a^*, b^*, c^*)$ of this model can be calculated by solving $\frac{da}{d\tau} = \frac{db}{d\tau} = \frac{dc}{d\tau} = 0$ simultaneously for (a, b, c), which becomes

$$(a^*, b^*, c^*) = (\alpha_0, \frac{\alpha_0 \tilde{\alpha}_1}{\alpha_0 + 1} - 1, \frac{1}{\tilde{\alpha}_1}).$$

To obtain a linear model around this steady state, we compute the Jacobian matrix and evaluate it at this steady state, which yields

$$J^*(a^*, b^*, c^*) = \begin{pmatrix} \frac{\partial g_a}{\partial a} & \frac{\partial g_a}{\partial b} & \frac{\partial g_a}{\partial c} \\ \frac{\partial g_b}{\partial a} & \frac{\partial g_b}{\partial b} & \frac{\partial g_b}{\partial c} \\ \frac{\partial g_c}{\partial a} & \frac{\partial g_c}{\partial b} & \frac{\partial g_c}{\partial c} \end{pmatrix}_{(a^*, b^*, c^*)} = \begin{pmatrix} -1 & 0 & 0 \\ 0 & 0 & \frac{\alpha_0 \tilde{\alpha}_1}{(\alpha_0+1)} - 1 \\ \frac{1}{(\alpha_0+1)\alpha_0 \tilde{\alpha}_1} & -\frac{(\alpha_0+1)}{\alpha_0\, \tilde{\alpha}_1^2} & -1 \end{pmatrix}$$

Similar to the IFFL model, after defining new variables defining deviations of dimensionless variables from their respective steady sate values as $\Delta a = a - a^*, \Delta b = b - b^*$ and $\Delta c = c - c^*$, the linear model approximating the local dynamics of the nonlinear model for the NFBL motif becomes

$$\begin{aligned}\frac{d\Delta a}{dt} =& - \Delta a\\ \frac{d\Delta b}{dt} =&\gamma_0 \Delta c\\ \frac{d\Delta c}{dt} =&\gamma_1 \Delta a + \gamma_2 \Delta b - \Delta c\end{aligned}$$

where $\gamma_0 = \frac{\alpha_0 \tilde{\alpha}_1}{(\alpha_0+1)} - 1, \gamma_1 = \frac{1}{(\alpha_0+1)\alpha_0 \tilde{\alpha}} > 0$ and $\gamma_2 = -\frac{(\alpha_0+1)}{\alpha_0 \tilde{\alpha}_1^2} < 0$. This model can be solved analytically to determine the local dynamics in the vicinity of the steady state.

Acknowledgements This work is partially supported by the New College of Florida Faculty Development Funds.

References

1. Mangan, S., Alon, U.: Structure and function of the feed-forward loop network motif. Proc. Natl. Acad. Sci. **100**(21), 11980–5 (2003)
2. Zhang, C., Tsoi, R., Wu, F., You, L.: Processing oscillatory signals by incoherent feedforward loops. PLoS Comput. Biol. **12**(9), e1005101 (2016)
3. Bretones, G., Delgado, M.D., León, J.: Myc and cell cycle control. Biochem. Biophys. Acta. (BBA)-Gene Regulatory Mechanisms **1849**(5), 506–16 (2015)
4. Lee, T., Yao, G., Nevins, J., You, L.: Sensing and integration of Erk and PI3K signals by Myc. PLoS Comput. Biol. **4**(2), e1000013 (2008)
5. Tsai, W.B., Aiba, I., Long, Y., Lin, H.K., Feun, L., Savaraj, N., et al.: Activation of Ras/PI3K/ERK pathway induces c-Myc stabilization to upregulate argininosuccinate synthetase, leading to arginine deiminase resistance in melanoma cells. Can. Res. **72**(10), 2622–33 (2012)
6. Ferrell, J.E.: Perfect and near-perfect adaptation in cell signaling. Cell Syst. **2**(2), 62–7 (2016)
7. Takeda, K., Shao, D., Adler, M., Charest, P.G., Loomis, W.F., Levine, H., et al.: Incoherent feedforward control governs adaptation of activated ras in a eukaryotic chemotaxis pathway. Science signaling. **5**(205), ra2-2 (2012)
8. Sasagawa, S., Yi, O., Fujita, K., Kuroda, S.: Prediction and validation of the distinct dynamics of transient and sustained ERK activation. Nat. Cell Biol. **7**(4), 365–73 (2005)
9. Lee, R.E., Walker, S.R., Savery, K., Frank, D.A., Gaudet, S.: Fold change of nuclear NF-κB determines TNF-induced transcription in single cells. Mol. Cell **53**(6), 867–79 (2014)
10. Adler, M., Alon, U.: Fold-change detection in biological systems. Current Opinion in Systems Biology. **8**, 81–9 (2018). (**Regulatory and metabolic networks Special Section: Single cell and noise**)
11. Goentoro, L., Shoval, O., Kirschner, M.W., Alon, U.: The incoherent feedforward loop can provide fold-change detection in gene regulation. Mol. Cell **36**(5), 894–9 (2009)
12. Tang, C., Ma, W., Trusina, A., El-Samad, H., Lim, W.: Defining network topologies that can achieve biochemical adaptation. FASEB J. **24**, 190–1 (2010)
13. Violin, J.D., DiPilato, L.M., Yildirim, N., Elston, T.C., Zhang, J., Lefkowitz, R.J.: β2-adrenergic receptor signaling and desensitization elucidated by quantitative modeling of real time cAMP dynamics. J. Biol. Chem. **283**(5), 2949–61 (2008)
14. Dohlman, H.G., Thorner, J.: RGS proteins and signaling by heterotrimeric G proteins. J. Biol. Chem. **272**(7), 3871–4 (1997)
15. Hao, N., Yildirim, N., Wang, Y., Elston, T.C., Dohlman, H.G.: Regulators of G protein signaling and transient activation of signaling: experimental and computational analysis reveals negative and positive feedback controls on G protein activity. J. Biol. Chem. **278**(47), 46506–15 (2003)
16. Semsey, S., Jauffred, L., Csiszovszki, Z., Erdőssy, J., Stéger, V., Hansen, S., et al.: The effect of LacI autoregulation on the performance of the lactose utilization system in escherichia coli. Nucleic Acids Res. **41**(13), 6381–90 (2013)
17. Yildirim, N., Mackey, M.C.: Feedback regulation in the lactose operon: a mathematical modeling study and comparison with experimental data. Biophys. J . **84**(5), 2841–51 (2003)
18. Harris, S.L., Levine, A.J.: The p53 pathway: positive and negative feedback loops. Oncogene **24**(17), 2899–908 (2005)
19. Mika, D., Richter, W., Conti, M.: A CaMKII/PDE4D negative feedback regulates cAMP signaling. Proc. Natl. Acad. Sci. **112**(7), 2023–8 (2015)
20. Rosenfeld, N., Elowitz, M.B., Alon, U.: Negative autoregulation speeds the response times of transcription networks. J. Mol. Biol. **323**(5), 785–93 (2002)
21. Perrimon, N., McMahon, A.P.: Negative feedback mechanisms and their roles during pattern formation. Cell **97**(1), 13–6 (1999)
22. Alon, U.: An introduction to systems biology: design principles of biological circuits. Chapman and Hall/CRC; (2006)

23. Ryzowicz, C., Yildirim, N.: Differential roles of transcriptional and translational negative autoregulations in protein dynamics. Molecular Omics. **19**(1), 60–71 (2023)
24. Alon, U.: Network motifs: theory and experimental approaches. Nat. Rev. Genet. **8**(6), 450–61 (2007)
25. Glass, L., Mackey, M.: Mackey-glass equation. Scholarpedia. **5**(3), 6908 (2010)
26. Mackey, M.C., Santillán, M., Yildirim, N.: Modeling operon dynamics: the tryptophan and lactose operons as paradigms. C.R. Biol. **327**(3), 211–24 (2004)
27. Santillán, M., Mackey, M.C.: Dynamic regulation of the tryptophan operon: a modeling study and comparison with experimental data. Proc. Natl. Acad. Sci. **98**(4), 1364–9 (2001)
28. Shi, W., Ma, W., Xiong, L., Zhang, M., Tang, C.: Adaptation with transcriptional regulation. Sci. Rep. **7**(1), 1–11 (2017)
29. Barkai, N., Leibler, S.: Robustness in simple biochemical networks. Nature **387**(6636), 913–7 (1997)
30. Shen-Orr, S.S., Milo, R., Mangan, S., Alon, U.: Network motifs in the transcriptional regulation network of escherichia coli. Nat. Genet. **31**(1), 64–8 (2002)
31. Maamar, H., Dubnau, D.: Bistability in the bacillus subtilis K-state (competence) system requires a positive feedback loop. Mol. Microbiol. **56**(3), 615–24 (2005)
32. Smits, W.K., Eschevins, C.C., Susanna, K.A., Bron, S., Kuipers, O.P., Hamoen, L.W.: Stripping bacillus: ComK auto-stimulation is responsible for the bistable response in competence development. Mol. Microbiol. **56**(3), 604–14 (2005)
33. Hahn, J., Kong, L., Dubnau, D.: The regulation of competence transcription factor synthesis constitutes a critical control point in the regulation of competence in Bacillus subtilis. J. Bacteriol. **176**(18), 5753–61 (1994)
34. Çağatay, T., Turcotte, M., Elowitz, M.B., Garcia-Ojalvo, J., Süel, G.M.: Architecture-dependent noise discriminates functionally analogous differentiation circuits. Cell **139**(3), 512–22 (2009)
35. Smits, W.K., Bongiorni, C., Veening, J.W., Hamoen, L.W., Kuipers, O.P., Perego, M.: Temporal separation of distinct differentiation pathways by a dual specificity Rap-Phr system in bacillus subtilis. Mol. Microbiol. **65**(1), 103–20 (2007)
36. Sun, Z., Wei, W., Zhang, M., Shi, W., Zong, Y., Chen, Y., et al.: Synthetic robust perfect adaptation achieved by negative feedback coupling with linear weak positive feedback. Nucleic Acids Res. **50**(4), 2377–86 (2022)
37. Frei, T., Khammash, M.: Adaptive circuits in synthetic biology. Current Opinion in Systems Biology. **28**, 100399 (2021)
38. Boyce, W.E., DiPrima, R.C., Meade, D.B.: Elementary differential equations and boundary value problems. John Wiley & Sons, United States (2021)
39. Iglesias, P.A., Shi, C.: Comparison of adaptation motifs: temporal, stochastic and spatial responses. IET Syst. Biol. **8**(6), 268–81 (2014)
40. Block, S.M., Segall, J.E., Berg, H.C.: Adaptation kinetics in bacterial chemotaxis. J. Bacteriol. **154**(1), 312–23 (1983)
41. Shimizu, T.S., Tu, Y., Berg, H.C.: A modular gradient-sensing network for chemotaxis in escherichia coli revealed by responses to time-varying stimuli. Mol. Syst. Biol. **6**(1), 382 (2010)
42. Wang, C.J., Bergmann, A., Lin, B., Kim, K., Levchenko, A.: Diverse sensitivity thresholds in dynamic signaling responses by social amoebae. Science signaling. **5**(213), ra17-7 (2012)

Publisher's Note Springer Nature remains neutral with regard to jurisdictional claims in published maps and institutional affiliations.

Springer Nature or its licensor (e.g. a society or other partner) holds exclusive rights to this article under a publishing agreement with the author(s) or other rightsholder(s); author self-archiving of the accepted manuscript version of this article is solely governed by the terms of such publishing agreement and applicable law.